ウェブサイト公開用

（様式 10）
（海外特別研究員事業）
令和　3 年　4 月　28 日

海 外 特 別 研 究 員 最 終 報 告 書

独立行政法人日本学術振興会 理事長　殿

採 用 年 度　2019
受 付 番 号　201960599
氏　　名　寺田　慧

（氏名は必ず自署すること）

海外特別研究員としての派遣期間を終了しましたので、下記のとおり報告いたします。
なお、下記及び別紙記載の内容については相違ありません。

記

1. 用務地（派遣先国名）用務地：　ニューヨーク　（国名：　米国　）

2. 研究課題名（和文）※研究課題名は申請時のものと違わないように記載すること。
複合記録系を用いたリップル再現発火中の BDNF 分泌による記憶固定化機構の解明

3. 派遣期間：平成　31 年　4 月　1 日　～　令和　3 年　3 月　31 日

4. 受入機関名及び部局名
受入機関名：the Mortimer Zuckerman Mind Brain and Behavior Institute at Columbia University
部局名：　Attila Losonczy Laboratory

5. 所期の目的の遂行状況及び成果…書式任意　**書式任意（A4 判相当 3 ページ以上、英語で記入も可）**
（研究・調査実施状況及びその成果の発表・関係学会への参加状況等）
（注）「6. 研究発表」以降については様式 10－別紙 1～4 に記入の上、併せて提出すること。

次ページより

・透過性グラフェン電極膜を用いて、 数千の海馬 CA1 錐体細胞の活動を ２光子イメージング で可視化しながら、それらの電気信号を計測することに成功した（in vivo 複合記録系の確立） 。
・通説を覆し、 C A1 リップル鋭波 が解剖学的特徴を反映した進行波であることを発見した。
・リップル鋭波の進行方向は、CA1 錐体細胞群の活動から予測することが可能である。
・現在、本プロジェクトの研究成果をまとめた論文を執筆している。

・in vivo 単一細胞電気穿孔法によって、麻酔下マウスの CA1 錐体細胞に BDNF-SEP の導入に成功した。しかし、COVID-19 蔓延防止の措置として、市内ロックダウンに伴い研究所が閉鎖され、半年以上にわたり研究活動の停止を余儀なくされた。そのため、本実験は断念して、上記および後述のプロジェクトを完遂することに注力した。

・in vivo 複合記録系を用いて、CA1 リップル鋭波中のシナプス前終末（CA3 Schaffer 側枝, CA3SC）の活動動態を長期間にわたり計測した（Figure. 1a)。
・記憶形成に伴うシナプス前終末の機能的変化を初めて観測することに成功した。
・CA3SC は、ランダムに呈示される新奇な感覚刺激に対して、柔軟に発火率を増加させることで、刺激応答性を獲得する（Figure. 1b)。
・これら Cue CA3SC は、逆にリップル鋭波中においては発火率を減少させるように変化させており、記憶固定化に関する再活性化から除外されていることが示唆された（Figure.1c & d)。
・一方で、感覚刺激がランダムではなく空間情報に関連付けられた場合においては（感覚-場所の連合記憶)、Cue CA3SC はリップル鋭波内での発火率を増加させており、再活性化されていることが分かった（Figure. 2)。
・この時、リップル鋭波中での Cue CA3SC の活動は、記憶学習中に観察された時系列パターンを繰り返し再活性化させていることが分かった（シナプス前終末のリップル再現発火、Figure. 3)。
・以上の結果から、CA1 へのシナプス入力は、多様な刺激情報を発火率増加によって符号化する一方で、その中から特定の情報だけを選択的に再活性化させていることが示唆された。これらの研究成果をまとめた論文を nature に投稿しており、現在、査読者と編集者の指示を反映したリバイス（修正）を行っている。

Reorganization of Schaffer Collateral inputs to the CA1 circuit during Associative Learning and CA1 sharp-wave ripples

Spatial and episodic memories guide adaptive behaviors in environmental contexts. The hippocampus forms contextual representations by selectively incorporating informative sensory features of the environment, but must somehow exclude behaviorally irrelevant distractors from memory consolidation. We investigated this selectivity conjecture using simultaneous calcium imaging and local field potential recordings in mice at CA3 Schaffer collaterals (CA3SC), the main excitatory pathway of the hippocampal circuitry.

Here, we report that the activity dynamics of CA3SCs during sensory experience and subsequent awake SWRs flexibly switches between two distinct modes of operation depending on the navigational relevance of sensory stimuli. As animals explore the environment during the memory acquisition phase, CA3SCs rapidly reorganize their activity dynamics to represent novel stimuli. Subsequently however, during SWR-associated reactivation and replay, only activity patterns that convey task-relevant sensory-spatial associations are reinstated while other patterns without navigational information are strongly suppressed.

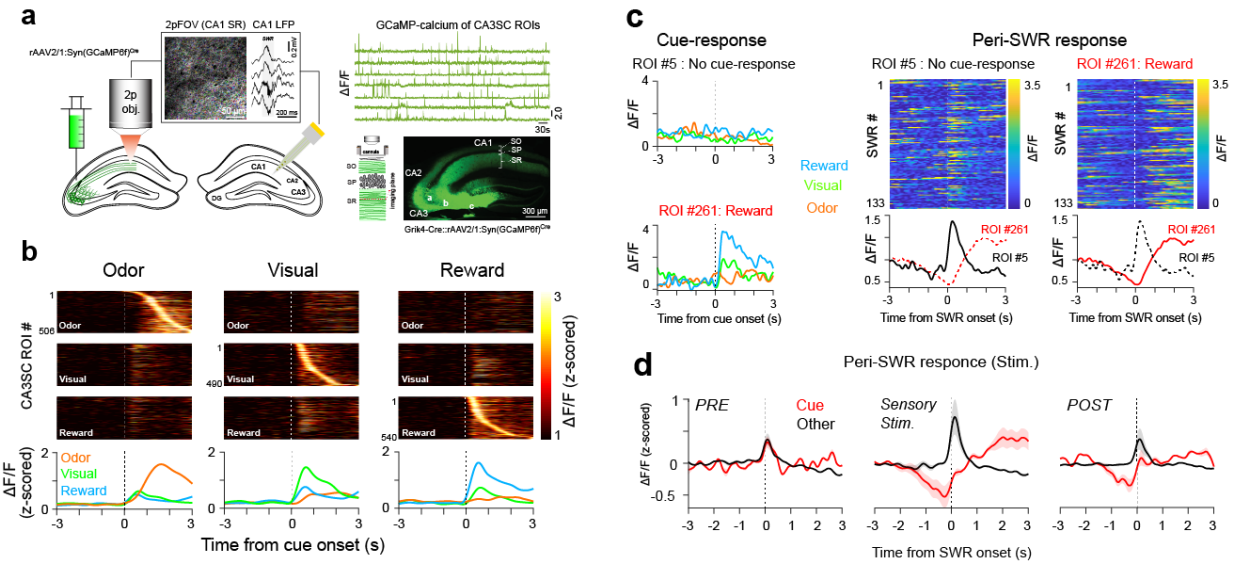

Figure 1. a, Left, schematic of simultaneous axonal two-photon (2p) imaging of hippocampal CA3 Schaffer collaterals (CA3SCs) in ipsilateral CA1 and local field potential (LFP) recordings. CA3 rAAV2/1:Syn(GCaMP6f)Cre injection was followed by implantation of a cannulated imaging window over ipsilateral CA1 and a 4-channel linear silicon probe in contralateral CA1. Box: example time-averaged 2p imaging field-of-view (2pFOV) with color dots showing detected ROIs from CA1 stratum radiatum (CA1 SR, left, note that ROIs were not cross-registered across days) and a representative example of a CA1 sharp wave ripple (SWR) detected on 4-channels (right, gray rectangle). Right top, representative relative GCaMP-calcium fluorescence (ΔF/F) traces extracted from CA3SCs ROIs. Right bottom, imaging schematics in CA1 and example coronal section of a Grik4-Cre mouse dorsal hippocampus showing rAAV-driven GCaMP6f expression in area CA3 encompassing all CA3 subregions (CA3a-c) and its CA3SC projection to CA1 (SO: stratum oriens, SP: stratum pyramidale, SR: stratum radiatum). **b**, Heatmap of trial-averaged peristimulus time histogram (PSTH) of identified cue-CA3SCs (all mice) during Random-Cue trials, ordered according to peak response time relative to cue onset. Cue-CA3SCs responding to multi-sensory cues are plotted for each modality. **c**, Sensory- and SWR-related activity profiles of two representative CA3SC ROIs recorded simultaneously. Cue-evoked average PSTHs during Random-Cue trials (top), heatmap (middle) and PSTH (bottom) of peri-SWR activity for SWRs detected during inter-stimulus intervals. **d**, mean peri-SWR response ± s.e.m. of all cue-CA3SCs (Cue, red) and non-cue CA3SCs (Other, black) recorded during Random-Cue trials (cue-CA3SCs, n=1219; other, n=5836, n=6 mice). Sensory cue presentation during Random-Cue trials (Sensory Sim.) was preceded (PRE) and followed by (POST) 15-min periods without sensory stimulation with continuous imaging of the same ROIs.

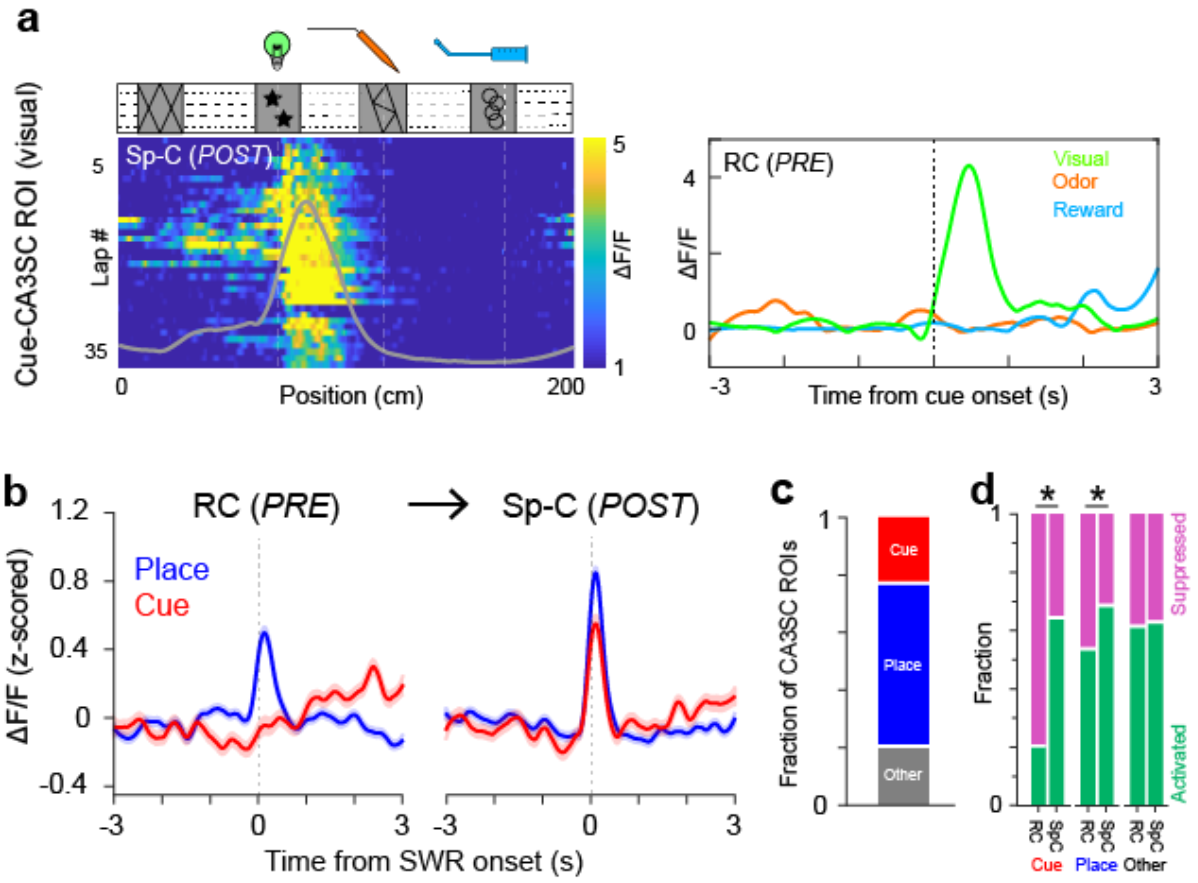

Figure 2. **a**, Left, lap-by-lap ΔF/F of a representative visual cue-CA3SC during Spatial-Cue trials (Sp-C). Right, mean preferred cue PSTH of the same ROIs during the preceding Random-Cue trials (RC). **b**, peri-SWR response (mean ± s.e.m) of cue-CA3SCs (red) and place-CASCs (blue) during RC (PRE) and Sp-C (POST). **c**, Fraction of cue-, place- and other CA3SC ROIs on Day 5. Each color indicates classified CA3SC ROI populations (red: cue, n=470, 22.9%; blue: place, n=1170, 56.8%; gray: other, n=418, 20.3%; from n=3 mice). d, peri-SWR response (mean ± s.e.m) of cue-CA3SCs (red) and place-CASCs (blue) during RC (PRE) and Sp-C (POST). **d**, Fraction of SWR recruitment of CA3SCs in RC-NS (PRE) and FC-S (POST, Day 5). Cue- and place-CA3SCs showed significantly different distributions of SWR recruitment between the conditions (Cue: RC, 20.4% activated, 79.6% suppressed; Sp-C, 64.5% activated, 35.5% as suppressed, $p<0.0001$. Place: RC, 53.8% activated, 46.2% suppressed; Sp-C, 68.6% activated, 31.4% suppressed, $p<0.001$. Other: RC, 61.5% activated, 38.5% suppressed; Sp-C, 62.9% activated, 37.1% suppressed, $p=0.7214$. Fisher's exact test).

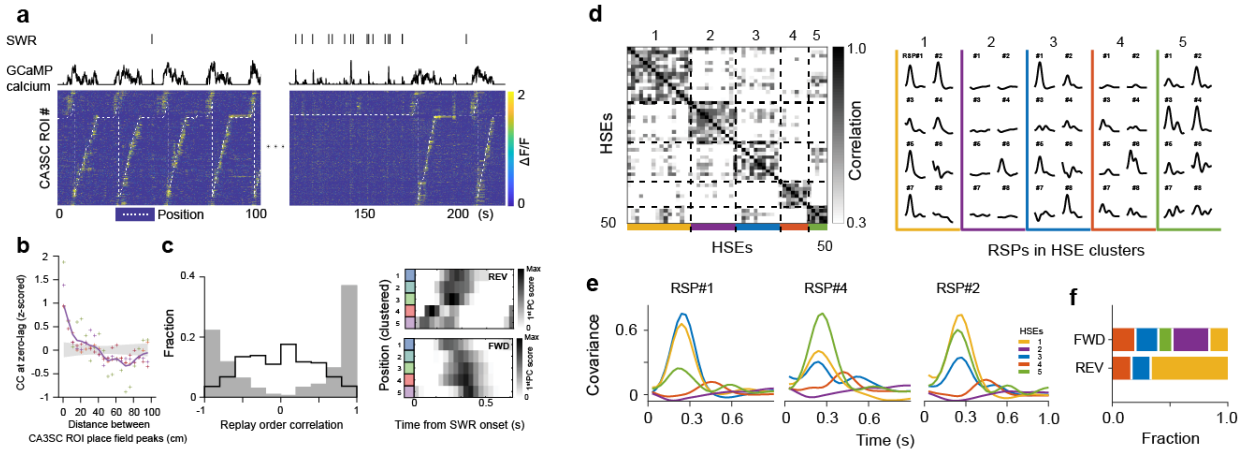

Figure 3. **a**, sequential activity of CA3SCs within a field-of-view for place coding during a running interval. Rows represent individual ROIs and white dashed line indicates mouse position. Onset of detected SWRs (black ticks) and mean CA3SC population activity (high synchrony event, HSE) are plotted above. **b**, Normalized cross-correlation (CC) at zero lag between all pairs of CA3SCs ROIs with place fields in Sp-C. The horizontal axis indicates pairwise distance between pairs of CA3SC place field peaks. Symbol styles denote individual mice (n=4 mice); purple line denotes average CC across mice. Gray shaded area indicates 97.5% confidence interval of CCs calculated from shuffled CA3SC pairs. **c**, Left, distribution of identified (gray bars) and shuffled (black line) replay order correlation. Right, two representative reverse (REV) and forward (FWD) replay events (color-coded grouping of CA3SCs based on place field location). **d**, Left, similarity map of all HSEs in a representative session sorted by recruitment of recurring synchronized populations (RSPs). Right, reactivated assemblies in each HSE cluster as combinatorial patterns of RSP participations. Colored lines tagged with ID numbers correspond with those in the similarity map. **e**, Examples of normalized covariance with HSE transients of three of the above RSPs. Note the different manners of SWR recruitment in each RSP. Ward's method was used to classify SWR-associated HSEs by these RSP participation patterns. Some RSPs were shared by several HSE clusters. Others participated in specific HSE clusters. **f**, Fraction of HSE clusters in significant FWD and REV replay events. We observed biased distribution of replay order between these HSE clusters, and if the distribution was significantly biased from the resampled distribution determined by shuffling, the clusters were classified into FWD-preferring or REV-preferring HSE clusters. In this session, two FWD-preferring (purple and green) and one REV-preferring clusters (yellow) were identified with the rest showing uniform distributions of replay sequences.